Two-Dimensional Line Shapes Derived from Coherent Third-Order Nonlinear Spectroscopy

Andrei Tokmakoff†

Department of Chemistry, Massachusetts Institute of Technology, Cambridge, Massachusetts 02139

Received: September 10, 1999; In Final Form: November 3, 1999

Two-dimensional (2D) line shapes derived from four types of coherent third-order nonlinear spectroscopies as a function of two independent time or frequency variables are compared. The signals scattered into two wave-vector-matching directions in the limits of high-time or high-frequency resolution are calculated for an inhomogeneously broadened ensemble of two-level systems with phenomenological dephasing and population relaxation times. While one-dimensional (1D) line shape analysis for this model is ambiguous, the contours of these 2D line shapes are shown to be characteristic of the relative time scales of the three relevant line-broadening parameters. These broadening mechanisms are also apparent by comparing 2D spectral profiles along the diagonal and antidiagonal frequency axes. For time domain experiments, in analogy with NMR correlation spectroscopy, the radiated signal is observed as a function of the two coherence periods and is 2D Fourier transformed to obtain a line shape. For experiments based on the photon echo, the ellipticity of the absolute value 2D line shape is related to the ratio of the inhomogeneous width to the dephasing rate, whereas experiments based on the transient grating method are shown to be functionally 1D. For frequency domain experiments, the contours of the 2D line shape can yield information on static and both dynamic broadening mechanisms. While the addition of spectral diffusion to such calculations will modify these results for frequency domain experiments, characterizing these dynamics in the time domain naturally leads to a 3D experiment analogous to the spin diffusion experiment in NMR.

Introduction

Describing the dynamics of amorphous condensed phases requires sensitivity to molecular motions and interactions on multiple time scales. Nonlinear spectroscopic methods are proving to be unusually discriminating for separating and quantifying the time scales of molecular and collective dynamics in systems such as liquids and solutions, supercooled liquids and glasses, polymers, and proteins. Of these methods, the most selective to dynamics of differing nature or with variable time scale are those that can peer beneath the ensemble average, such as hole burning and the photon echo.

Although these are well-understood experiments, control of the multiple time variables inherent to these third-order spectroscopic methods is still elusive. Hole-burning measurements are sensitive to the time scale of burning and the time between reading and burning.[1,2] Control over these variables allows the dynamics of spectral diffusion to be monitored. Although selective to the fast dynamics in inhomogeneously broadened systems, the traditional two-pulse photon echo is not particularly sensitive to the dynamics of systems with a broad distribution of time scales. This realization led to the use of multiple time variables in the photon echo experiment to get at spectral diffusion. These experiments include stimulated photon echo experiments[1,3] and the three-pulse photon echo peak shift measurement.[4−6] It has been realized that observing the time evolution of the radiated polarization holds much of the information on the time scales and mechanism over which memory of an initial excitation is lost. This is the motivation for experiments such as the gated photon echo,[7,8] heterodyne-detected photon echo,[9,10] and fifth-order three-pulse echo.[11,12]

These techniques are now being used as the template for the development of even more insightful two-dimensional (2D) electronic[13−15] and vibrational[16−25] spectroscopies. These 2D spectroscopies are in many ways optical analogues of 2D correlation spectroscopies used in nuclear magnetic resonance (NMR);[26] they attempt to observe microscopic interactions through macroscopic correlations between differing spectroscopic features. What is particularly appealing is the time scale over which these measurements can be made: as short as a few tens of femtoseconds.

2D spectroscopies are those observed as a function of two independent time or frequency variables, and thereby they can be related to correlation functions in two time variables (three-point correlation functions). Whether they are observed in time or frequency, observables are most often presented as a 2D spectrum, which represents the correlation between spectroscopic features. The 2D spectrum has an amplitude and phase spectrum associated with it. The amplitude is a measure of the degree of correlation, which can refer to the strength of coupling of two modes or the extent of spectral diffusion between two transition energies. The phase offers a new level of information on the correlation. It can be used to assist in distinguishing the mechanism of coupling, describing the momentum of electronic and vibrational wave packets, and separating dynamics on the ground and excited electronic surfaces.

Our aim in this paper is to illustrate how 2D line shape analysis of features in a 2D spectrum has the ability to separate different dynamic and static contributions to a molecular dipole transition. While one-dimensional (1D) line shapes based on optical, infrared, or Raman spectroscopy cannot unambiguously separate fast and slow dynamics or dynamics of dephasing and population relaxation, 2D line shapes can.[13,19,27] Resonant third-order nonlinear spectroscopies can be related to correlation

† E-mail: tokmakof@mit.edu. Fax: (617) 253-7030.

10.1021/jp993207r CCC: $19.00
Published on Web 12/16/1999

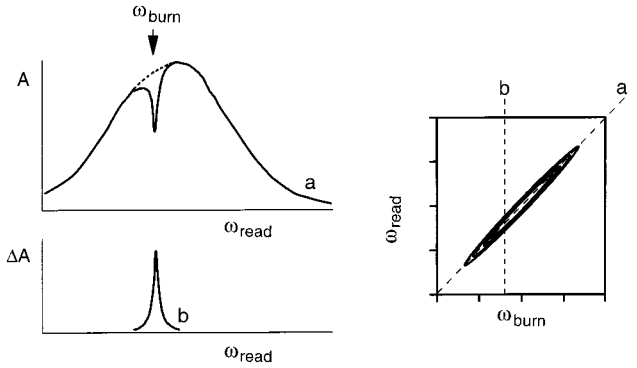

Figure 1. Schematic of a two-dimensional experiment based on hole burning. A narrow bandwidth burning pulse at ω_{burn} bleaches an inhomogeneously broadened transition. The differential absorption derived from a scan of the line shape before and after the bleach by ω_{read} yields a slice (b) from the 2D line shape. Tuning both frequencies allows a 2D line shape to be constructed. The diagonal slice (a) of this spectrum reproduces the absorption line shape. The pictured line shape is representative of a system with an invariant homogeneous width across the distribution. If it were frequency dependent, then shapes such as those in Figure 6a would be expected.

functions in three time variables.[28] Time ordering of pulses, frequency selection of the interaction fields, wave-vector-matching conditions, and polarization conditions allow an experiment to be designed that is selective to the form of these correlation functions. Here we use selectivity by wave vector, time-ordering, and frequency to illustrate which microscopic variables 2D line shapes can be sensitive to.

The manner in which dynamic information can be extracted from 2D line shapes can be illustrated by the 2D representation of a traditional hole-burning experiment on an inhomogeneously broadened absorption line. As shown in Figure 1, a subset of the ensemble can be photobleached by an intense monochromatic field with a frequency ω_{burn}. The induced change in the absorption line shape is measured by a weak read-out beam at frequency ω_{read}. For a distribution of homogeneous line shapes masked by inhomogeneous broadening, the difference spectrum is representative of the homogeneous line shape of the subensemble absorbing at ω_{burn}. This experiment is a function of two independent frequency variables, and is thus two-dimensional. If we now allow both ω_{burn} and ω_{read} to be tuned through the inhomogeneous line shape, we can construct a 2D line shape as a function of these two variables. This line shape will have an elliptical line shape whose profile along the diagonal frequency axis ($\omega_{burn} = \omega_{read}$) reproduces the traditional 1D absorption spectrum. The width perpendicular to the diagonal represents the homogeneous line width. The ellipticity of the line tells about the extent of inhomogeneous broadening. These observations suggest that the 2D line shape, in addition to giving a quantitative description of multiple time scales, allows tremendous intuitive insight into the nature of spectral broadening and the makeup of the ensemble.

The following calculations aim to demonstrate the information content on spectral broadening mechanisms found in 2D line shapes, as derived from four types of coherent third-order nonlinear spectroscopies. Using a phenomenological Bloch model for a two-level system (2LS), 2D line shapes are derived for signals observed in two phase-matching conditions in the limit of high-time or high-frequency resolution. These calculations show the complementary nature of these experiments in extracting dynamic information on the system. In each case, as with the example in Figure 1, the shapes of the contours that represent the 2D line shape are uniquely representative of the time scales of the dynamics. Time domain experiments are selective to the influence of static (inhomogeneous) broadening, while frequency domain experiments are sensitive to the ratio of the rates of dephasing to population relaxation. To demonstrate the sensitivity of 2D spectroscopies to the makeup of the ensemble beyond traditional means, a system with a frequency-dependent dephasing time is investigated. These examples also serve to build intuitive analysis of 2D line shapes by demonstrating how 2D line shapes allow a simplified representation of the dynamics of a complex system. By designing the experiment with varying degrees of time or frequency resolution and wave-vector selection, different types of information can be extracted from the system. Further, these calculations demonstrate the remarkable ability of 2D observables to lend tremendous qualitative and quantitative insight into the dynamics of ensembles.

TABLE 1: Resonant Third-Order Nonlinear Experiments on a Two-Level System with Two Independent Time or Frequency Variables[a]

case	independent variables	wavevector matching condition	frequency conservation condition
I	τ_1, τ_3	$k_{PE} = -k_1 + k_2 + k_3$	$\omega_{PE} = -\omega_1 + \omega_2 + \omega_3$
II	τ_1, τ_3	$k_{TG} = +k_1 - k_2 + k_3$	$\omega_{TG} = +\omega_1 - \omega_2 + \omega_3$
III(a)	$\omega_1 = \omega_2, \omega_3$	$k_{PE} = -k_1 + k_2 + k_3$	$\omega_{PE} = -\omega_1 + \omega_2 + \omega_3$
(b)	$\omega_1, \omega_2 = \omega_3$		
(c)	$\omega_1 = \omega_3, \omega_2$		
IV(a)	$\omega_1 = \omega_2, \omega_3$	$k_{TG} = +k_1 - k_2 + k_3$	$\omega_{TG} = +\omega_1 - \omega_2 + \omega_3$
(b)	$\omega_1, \omega_2 = \omega_3$		
(c)	$\omega_1 = \omega_3, \omega_2$		

[a] Of these, there are four independent experiments, when considering the following symmetries: case IIIa = case IVa; case IIIb = case IVc; case IIIc = case IVb; case IIIa, $S(\omega_1,\omega_3)$ = case IVb, $S(\omega_3,\omega_1)$ (reflection symmetry).

Calculations

To illustrate the information content of various 2D line shapes based on coherent third-order resonant nonlinear spectroscopy, we calculate the 2D response from four types of experiments. The description of the response from an ensemble of 2LSs in the limits of high-time or high-frequency resolution leads to the four 2D experiments outlined in Table 1. Two experiments are measured in the time domain, and two are measured in the frequency domain. For each domain, we consider two wave-vector-matching conditions, $k_{PE} = -k_1 + k_2 + k_3$, the photon echo (PE) wave-vector-matching condition, and $k_{TG} = +k_1 - k_2 + k_3$, the wave-vector-matching condition for transient grating (TG), pump−probe, or hole-burning experiments. For the time domain experiments we calculate an observable in the two time variables τ_1 and τ_3, the first and last time variables associated with the four-point correlation functions that describe third-order nonlinear experiments.[28] For an optical 2LS, these time periods are those during which the system evolves in coherences. Most nonlinear experiments would not measure such an observable, since traditional detection integrates over τ_3, yet heterodyne detection and gating of the τ_3 signal are potential methods for such an observation.[7−10] For frequency domain 2D experiments, we choose two independent frequency variables for the input fields and set the third equal to one of the others. This constraint dictates that only two distinct experiments exist after consideration of the symmetry of the frequency variables. In this case, no time-ordering is retained, and the response is obtained by summing over all possible interaction pathways. We use an ensemble of 2LSs consisting of a ground state $|g\rangle$ and an excited state $|e\rangle$ split by a frequency $\omega_{eg} = \omega_e - \omega_g$. The damping of

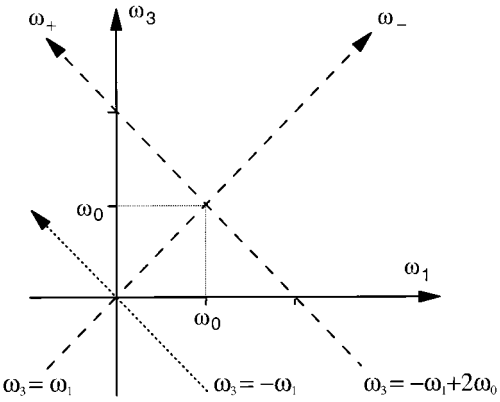

Figure 2. Relationship between the frequency variables from Fourier transformation of the response function time variables and the rotated axis frame of the diagonal (ω_-) and antidiagonal (ω_+) axes.

the 2LS is governed by two phenomenological constants for the dephasing rate $\Gamma_{eg} = \Gamma_{ge}$ and population relaxation $\Gamma_{ee} = \Gamma_{gg}$.

As illustrated by the example in Figure 1, the dimensions that most clearly describe a 2D spectrum are the diagonal and antidiagonal axes. The diagonal axis, in which the two frequency arguments are the same ($\omega_{read} - \omega_{burn} = 0$), is usually representative of the information in a 1D experiment. The antidiagonal axis, which satisfies the relationship $\omega_{read} + \omega_{burn} = 2\omega_0$, is perpendicular to the diagonal at the point (ω_0,ω_0) in the 2D plane. As a first level of characterization, the shape of the line can be described by comparing the width along these two axes. More generally, these two primary axes represent a translation of the origin to (ω_0, ω_0) and rotation of the axis frame by 45°. In the following, for an observable in two frequency variables, ω_1 and ω_3, the diagonal frequency variable will be defined as

$$\omega_- = \omega_3 - \omega_1 \tag{1}$$

and the antidiagonal as

$$\omega_+ = \omega_1 + \omega_3 - 2\omega_0 \tag{2}$$

These axes are pictured in Figure 2. These definitions, which neglect a factor of $1/\sqrt{2}$ for rotation of the axes, are chosen to retain a direct relationship between the shape and width of spectral features in the 2D plane, and their 1D counterparts.

Time Domain Experiments. We first consider two four-wave mixing experiments in which three successive optical pulses are directed at the sample, in which the time variables for the separation between successive pulses are τ_1 and τ_2, and τ_3 is the time period after the final field interaction. The pulses are considered short compared with the dynamics, yet long compared with the optical cycle. For the case of third-order nonlinear experiments within the rotating wave approxiation, the signal radiated during τ_3 by the nonlinear polarization, $P^{(3)}$, is a convolution of the input fields over the third-order response function $R^{(3)}$ [28]

$$P^{(3)}(\tau_1,\tau_2,\tau_3) \propto \int_0^\infty d\tau_3 \int_0^\infty d\tau_2 \int_0^\infty d\tau_1\, R^{(3)}(\tau_1,\tau_2,\tau_3) \times \bar{E}_3(\tau-\tau_3)\, \bar{E}_2(\tau-\tau_3-\tau_2)\, \bar{E}_1(\tau-\tau_3-\tau_2-\tau_1) \tag{3}$$

where the third-order response function is given by a sum of four time-ordered, frequency- and wave-vector-matched contributions

$$R^{(3)}(\tau_1,\tau_2,\tau_3) = (i/\hbar)^3\, \theta(\tau_1)\, \theta(\tau_2)\, \theta(\tau_3) \sum_{i=1}^{4} (R_i(\tau_1,\tau_2,\tau_3) - R_i^*(\tau_1,\tau_2,\tau_3)) \tag{4}$$

with

$$R_1(\tau_1,\tau_2,\tau_3) = \exp(-i\omega_{eg}\tau_1 - i\omega_{eg}\tau_3) \exp(-g^*(\tau_3) - g(\tau_1) - g^*(\tau_2) + g^*(\tau_2+\tau_3) + g(\tau_1+\tau_2) - g(\tau_1+\tau_2+\tau_3)) \tag{5a}$$

$$R_2(\tau_1,\tau_2,\tau_3) = \exp(i\omega_{eg}\tau_1 - i\omega_{eg}\tau_3) \exp(-g^*(\tau_3) - g^*(\tau_1) + g(\tau_2) - g(\tau_2+\tau_3) - g^*(\tau_1+\tau_2) + g^*(\tau_1+\tau_2+\tau_3)) \tag{5b}$$

$$R_3(\tau_1,\tau_2,\tau_3) = \exp(i\omega_{eg}\tau_1 - i\omega_{eg}\tau_3) \exp(-g(\tau_3) - g^*(\tau_1) + g^*(\tau_2) - g^*(\tau_2+\tau_3) - g^*(\tau_1+\tau_2) + g^*(\tau_1+\tau_2+\tau_3)) \tag{5c}$$

$$R_4(\tau_1,\tau_2,\tau_3) = \exp(-i\omega_{eg}\tau_1 - i\omega_{eg}\tau_3) \exp(-g(\tau_3) - g(\tau_1) - g(\tau_2) + g(\tau_2+\tau_3) + g(\tau_1+\tau_2) - g(\tau_1+\tau_2+\tau_3)) \tag{5d}$$

Here $\theta(t)$ is the unit step function. The response functions can in turn be calculated from the line-broadening function $g(t)$ which describes the dynamics of the spectroscopic energy gap V

$$g(t) = (1/\hbar^2) \int_0^t d\tau \int_0^\tau d\tau' \, \langle V(\tau')\, V(0)\rangle \tag{6}$$

The line-broadening function can be related to a spectral density, $\rho(\omega)$, for the fluctuations in V. A detailed description of the evaluation of $P^{(3)}$ in terms of $g(t)$ and $\rho(\omega)$ can be found elsewhere.[28−30] By assuming short, well-separated pulses, we replace the electric field functions in eq 3 with δ function envelopes. Thus, the nonlinear polarization is proportional to $R^{(3)}$. Also for these calculations τ_2 is set to zero, so that $R_1 = R_4$ and $R_2 = R_3$. For the first set of calculations, our simple model is equivalent to the traditional Bloch picture, with

$$g(t) = \Gamma_{eg} t \tag{7}$$

leading to

$$R^{(3)}_{PE}(\tau_1,\tau_3) = R_2 + R_3 = \exp(-i\omega_{eg}(\tau_3 - \tau_1)) \exp(-\Gamma_{eg}(\tau_1 + \tau_3)) \tag{8}$$

$$R^{(3)}_{TG}(\tau_1,\tau_3) = R_1 + R_4 = \exp(-i\omega_{eg}(\tau_1 + \tau_3)) \exp(-\Gamma_{eg}(\tau_1 + \tau_3)) \tag{9}$$

Here all constant factors that influence the overall magnitude of the signal, but not its time dependence, have been dropped. We also include a slow dynamic time scale through inhomogeneous broadening, which is described as a Gaussian distribution of transition frequencies, ω_{eg}, with width σ

$$G(\omega_{eg}) = (2\pi\sigma^2)^{-1/2} \exp(-(\omega_{eg} - \omega_0)^2/2\sigma^2) \tag{10}$$

Here ω_0 is the center of the distribution. The time domain response for the ensemble is obtained by integrating the time domain response function over the inhomogeneous distribution

$$R^{(3)} = \int G(\omega_{eg})\, R^{(3)}(\omega_{eg})\, d\omega_{eg} \tag{11}$$

This leads to the well-known ensemble-averaged response function for the two time domain experiment:[28]

$$R^{(3)}_{PE}(\tau_1,\tau_3) = \exp(-\Gamma_{eg}(\tau_1+\tau_3))\exp(-(\tau_3-\tau_1)^2\sigma^2/2)\times \exp(-i\omega_0(\tau_3-\tau_1)) \quad (12)$$

$$R^{(3)}_{TG}(\tau_1,\tau_3) = \exp(-\Gamma_{eg}(\tau_1+\tau_3))\exp(-(\tau_3+\tau_1)^2\sigma^2/2)\times \exp(-i\omega_0(\tau_1+\tau_3)) \quad (13)$$

It is clear that this model does not address the dynamics of population relaxation and spectral diffusion, which are observed during τ_2. Observation of these dynamics can be measured with 3D experiments that observe the 2D spectrum as a function of τ_2, the population period in echo experiments and the mixing period in NMR experiments. Traditional observation of time domain third-order nonlinear signals makes an integrated measurement of the third-order polarization radiated from the sample

$$S^{(3)}(\tau_1,\tau_2) \propto \int_0^\infty |P^{(3)}|^2\, d\tau_3 \quad (14)$$

To construct the 2D experiments here using the two coherence periods τ_1 and τ_3, it is necessary to observe the electric field during the final period. Both gated photon echoes[7,8,31] and heterodyne-detected photon echoes[9,10] are designed for this purpose. It should be noted that spectral interferometry[32−34] is effectively equivalent to the heterodyne-detected method since both of these methods are capable of measuring the complex 3D polarization from third-order nonlinear measurements. For the 2D line shapes discussed here, only observation of the time envelope of the radiated polarization, $|P^{(3)}(\tau_1,\tau_3)|$, during the time τ_3 as a function of τ_1 is required. This makes the gated photon echo, which measures a signal proportional to $|P^{(3)}(\tau_1,\tau_3)|^2$ the most direct route to these line shapes.

Figure 3 shows the time domain envelopes of the 2D response for the PE and TG experiments from ensembles of varying inhomogeneous widths. As the inhomogeneous distribution becomes large compared to the homogeneous dephasing time, the PE experiment (Figure 3a−c) changes from a symmetric to a diagonally elongated signal. In the strongly inhomogeneous limit, an echo ridge arising from the rephasing term in eq 12 is observed. The decay along the diagonal is given by Γ_{eg}, while the decay along the time axes ($\tau_1 = 0$ or $\tau_3 = 0$) is a product of the exponential and Gaussian decays from the homogeneous and inhomogeneous dephasing mechanisms.

For the TG experiment, the signal is temporally uniform; it decays monotonically downward at the same rate in any direction in the two time variables. The rate of this falloff is governed by the fastest dephasing mechanism, whether homogeneous or inhomogeneous. Contours in the 2D plane are always of slope −1. As suggested by the diagonal and antidiagonal frequency variables (eqs 1 and 2), we can also define diagonal and antidiagonal axes in the time domain

$$\tau_- = \tau_3 - \tau_1 \quad (15)$$

$$\tau_+ = \tau_1 + \tau_3 \quad (16)$$

Rewriting the response functions for the PE and TG experiments

$$R^{(3)}_{PE}(\tau_+,\tau_-) = \exp(-\Gamma_{eg}\tau_+)\exp(-\tau_-{}^2\sigma^2/2)\exp(-i\omega_0\tau_-) \quad (17)$$

$$R^{(3)}_{TG}(\tau_+) = \exp(-\Gamma_{eg}\tau_+)\exp(-\tau_+{}^2\sigma^2/2)\exp(-i\omega_0\tau_+) \quad (18)$$

it becomes clear that the transient grating can be written in terms of one independent time variable, τ_+, and is thus functionally a one-dimensional experiment.

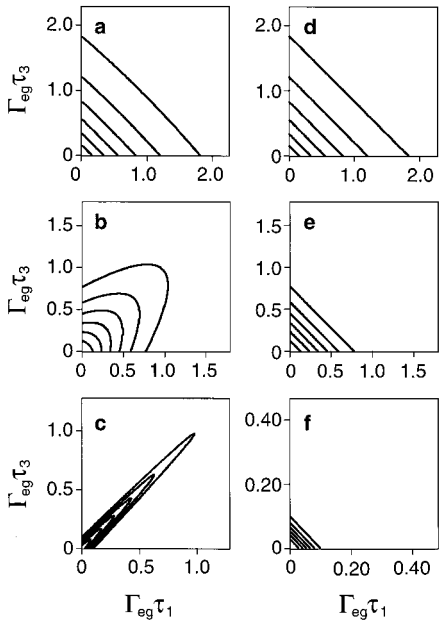

Figure 3. Two-dimensional contours of the time domain response, $|P^{(3)}(\tau_1,\tau_3)|$, for the PE (a−c) and TG (d−f) experiments from the homogeneous to the inhomogeneous limit: (a, d) $\sigma/\Gamma_{eq} = 0.2$; (b, e) $\sigma/\Gamma_{eq} = 2$; (c, f) $\sigma/\Gamma_{eq} = 20$. Contours are shown in intervals of 14% of the maximum amplitude.

With the observation of the amplitude of the third-order polarization as a function of the two time variables τ_1 and τ_3, as in the gated echo, we can define a 2D spectrum for these experiments through a two-dimensional Fourier transform

$$S(\omega_1,\omega_3) = \int_{-\infty}^{\infty} d\tau_1 \int_{-\infty}^{\infty} d\tau_3\, |P^{(3)}(\tau_1,\tau_3)| \exp(\pm i\omega_1\tau_1 + i\omega_3\tau_3) \quad (19)$$

The sign of the ω_1 frequency argument in the complex exponential is determined by the sign of these terms in the frequency and wave-vector-matching condition for the experiment, i.e., $-\omega_1$ for the PE and $+\omega_1$ for the TG. The spectrum is defined in this manner to show direct correspondence between time and frequency domain experiments. The choice of sign is otherwise arbitrary, since it only leads to rotation of the spectrum by 90°. It should be noted that the Fourier transform relationship in eq 19 can in principle be redefined in terms of the transform pair $\omega_+\tau_+$ and $\omega_-\tau_-$, but the change of integration limits is nontrivial.

The 2D line shapes obtained from the time domain response in Figure 3 are shown in Figure 4. These are absolute value spectra obtained from eq 19. As with the time domain response, the 2D line shape is very revealing in the PE experiment, yet hardly changes in profile for the TG experiment. In the homogeneous limit (Figure 4a), the 2D line shape from the PE is symmetric with the characteristic shape of a 2D Lorentzian.[26] As the inhomogeneous width increases, the 2D line shape broadens along the diagonal axis, while the antidiagonal is unchanged. For large inhomogeneous broadening (Figure 4c), the 2D line shape is strongly elongated, with the diagonal profile given by the inhomogeneous width and the antidiagonal axis still preserving the homogeneous line shape. In the Bloch model, the 2D line shape from the PE experiment is similar to that from the hole-burning experiment. Clearly in an inhomogeneous system, the ellipticity of the 2D line shape can be related to the degree of inhomogeneous broadening. This has been shown

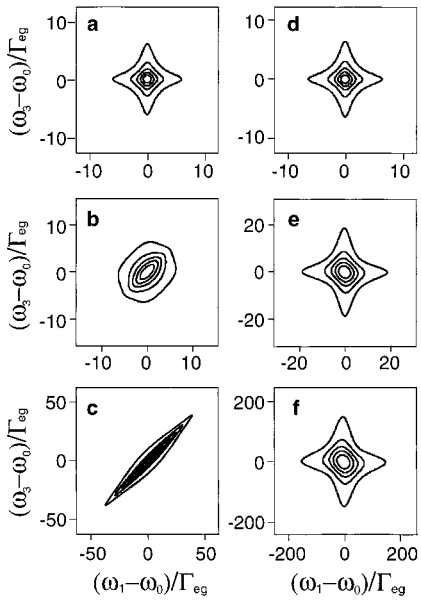

Figure 4. Two-dimensional absolute value line shapes, $|S(\omega_1,\omega_3)|$, obtained from the calculations in Figure 3 using eq 19. The labels a−f correspond to those in Figure 3. Contours are shown in 17% of the maximum intervals.

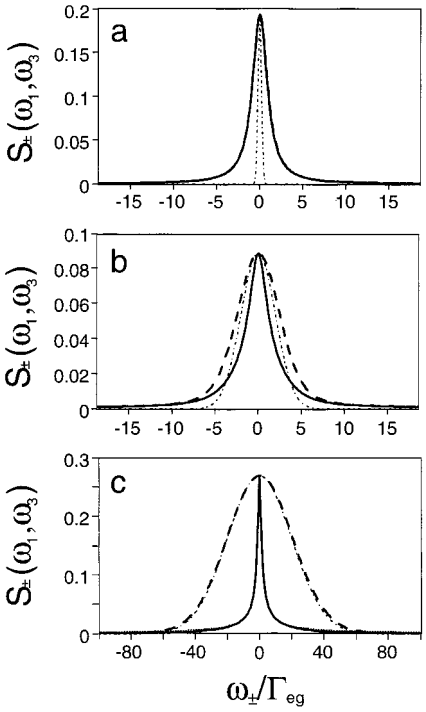

Figure 5. Diagonal (dashed line) and antidiagonal (solid line) slices through the 2D line shapes obtained from the PE experiment in Figures 3 and 4. The labels a−c correspond to Figures 3 and 4. The light dotted line illustrates the Gaussian inhomogeneous distribution in each case.

quantitatively elsewhere for the PE experiment.[27] Since the Bloch model for the photon echo experiment is effectively the same as that used for spin−echo experiments, the 2D line shapes derived here are similar to those described in the analysis of 2D NMR line shapes.[26]

Slices through the 2D spectra obtained from the PE experiment are shown in Figure 5. In general, the diagonal slice contains the information of the traditional 1D absorption experiment, a convolution of the homogeneous and inhomogeneous dephasing dynamics. (More precisely, the diagonal slice from the real part of the 2D line shape is the absorption

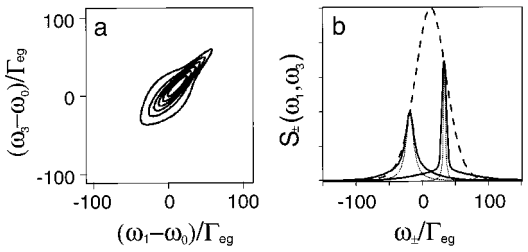

Figure 6. (a) 2D line shape, $|S(\omega_1,\omega_3)|$, obtained from a PE experiment for an inhomogeneous ensemble in which the homogeneous dephasing rate, Γ_{eg}, is frequency dependent ($\sigma/\Gamma = 20$; $\alpha = \Gamma/10$). (b) Diagonal (dashed line) and antidiagonal (solid line) slices through the 2D spectrum in (a). The antidiagonal slices ($\omega_+ = \omega_3 + \omega_1 - 2\omega_{eg}$) on either side of the distribution center, ω_0, are representative of the homogeneous line width at that frequency. For comparison, a Lorentzian line shape with width $\Gamma_{eg}(\omega_{eg})$ is shown.

spectrum.) In the homogeneous limit, the diagonal is given by the imaginary part of the Lorentzian line shape

$$S_-(\omega_-) \propto \Gamma/((\omega_- - \omega_{eg})^2 + \Gamma^2) \tag{20}$$

In the inhomogeneous limit, it is a Gaussian with the profile of the inhomogeneous distribution. The antidiagonal slice gives information on the homogeneous line shape. In the homogeneous limit ($\Gamma \gg \sigma$), the antidiagonal slice is identical to the diagonal slice (eq 20). In the inhomogeneous limit ($\sigma \gg \Gamma$), the antidiagonal slice is the modulus-squared Lorentzian

$$S_+(\omega_+) \propto 1/({\omega_+}^2 + \Gamma^2)^{1/2} \tag{21}$$

The projection of the 2D spectrum onto the antidiagonal for any values of σ and Γ is always given by eq 20 above. This is a consequence of the projection theorem that states that the Fourier transform of a time slice in the 2D plane—in our case the time diagonal—gives the projection onto that axis in the frequency domain—in our case the antidiagonal due to the definition used in eq 19.[26]

Within the simple model used above, the analysis of 2D experiments based on the absolute value of the electric field is essentially equivalent in the time or frequency domain. The choice of representation is arbitrary. The choice of time or frequency domain representation is less arbitrary in systems of increasing complexity. In systems that are composed of multiple distinct or superimposed components, the time domain response does not have the same intuitive interpretation that the 2D line shape has. As an illustration, consider an inhomogeneously broadened system in which the dephasing dynamics for the members of the ensemble is frequency dependent. This scenario could be observed for any frequency-dependent relaxation mechanism, such as relaxation through bath-mediated anharmonic coupling mechanisms. In this case, the homogeneous line shape is broader on one side than the other. If the homogeneous dephasing rate is linearly proportional to frequency

$$\Gamma_{eg} = \Gamma_0 - \alpha(\omega_{eg} - \omega_0) \tag{22}$$

then the PE response of the ensemble integrated over a Gaussian distribution function is given by

$$R^{(3)}_{PE}(\tau_1,\tau_3) = \exp(-\Gamma_0(\tau_1 + \tau_3)) \exp((-\sigma^2/2)(\alpha^2(\tau_1 + \tau_3)^2 + (\tau_3 - \tau_1)^2 - 2i\alpha({\tau_3}^2 - {\tau_1}^2))) \exp(-i\omega_0(\tau_3 - \tau_1)) \tag{23}$$

The 2D line shape observed for this system is shown in Figure 6a for $\sigma/\Gamma = 20$ and $\alpha = \Gamma/10$. The line shape is pear shaped

and symmetric about the diagonal axis. This shape characterizes the makeup of this ensemble effectively, as shown in Figure 6b. The diagonal axis again is representative of the 1D spectrum: an asymmetric line shape that represents the convolution of the frequency-dependent homogeneous line widths with the distribution function. The antidiagonal slice at any detuning from the center of the distribution, $\omega_{eg} - \omega_0$, is representative of the homogeneous line width of the members of the ensemble at that detuning. This qualitative interpretation is apparent from the 2D line shape, while the time domain representation is not as intuitive. Yet, for quantitative modeling the two representations contain the same information.

Frequency Domain Experiments. Next we consider 2D line shapes derived from frequency domain third-order nonlinear experiments. Three beams with wave vectors, k_1, k_2, and k_3, with frequencies ω_1, ω_2, and ω_3, and of bandwidth much narrower than the inverse of the dynamic time scales are used to generate a third-order nonlinear signal. This could apply to cw experiments or time-coincident pulses that are much longer than the dynamics. We analyze the nonlinear signal scattered in the same wave-vector-matching directions as before, the PE ($k_{PE} = -k_1 + k_2 + k_3$) and TG ($k_{TG} = +k_1 - k_2 + k_3$) geometries. As before, we will consider the line shape that is proportional to the magnitude of the polarization, $S(\omega_1,\omega_3) \propto |P^{(3)}(\omega_1,\omega_3)|$; this would be equivalent to the square root of the background free coherent signal observed by a photodetector. The frequency of the emitted signal is given by the conditions $\omega_{PE} = -\omega_1 + \omega_2 + \omega_3$ and $\omega_{TG} = +\omega_1 - \omega_2 + \omega_3$, respectively. As a simple example of a 2D experiment, we consider the case where one of the three independent frequencies is set equal to one of the others, i.e., $\omega_1 = \omega_2$, $\omega_2 = \omega_3$, or $\omega_1 = \omega_3$.

The frequency domain responses for these experiments have been written by many others.[35−39] From the standpoint of the correlation functions, the frequency domain response function, or susceptibility $\chi^{(3)}$, can be obtained by a Fourier transform relationship to the time domain response function:

$$\chi^{(3)}(-\omega_s;\omega_1,\omega_2,\omega_3) \propto \sum_{i,j,k=1,2,3} \int_0^\infty d\tau_3 \int_0^\infty d\tau_2 \times \int_0^\infty d\tau_1\, R^{(3)}(\tau_1,\tau_2,\tau_3) \exp(-i(\omega_i + \omega_j + \omega_k)\tau_3 - i(\omega_j + \omega_k)\tau_2 - i\omega_k\tau_1) \quad (24)$$

Within the 2LS model described above, the nonlinear susceptibility leading to the nonlinear signal with frequency $\omega_s = +\omega_1 - \omega_2 + \omega_3$, scattered into the PE wave-vector-matching direction, is described by a sum over all time-orderings

$$\chi^{(3)}(-\omega_s;-\omega_1,\omega_2,\omega_3) = \frac{2}{\omega_{eg} - (-\omega_1 + \omega_2 + \omega_3) - i\Gamma_{eg}}\left[\frac{1}{(-\omega_2 + \omega_1) - i\Gamma_{ee}} \times \left(\frac{1}{\omega_{eg} + \omega_1 - i\Gamma_{eg}} + \frac{1}{-\omega_{eg} - \omega_2 - i\Gamma_{eg}}\right) + \frac{1}{(-\omega_2 - \omega_3) - i\Gamma_{ee}}\left(\frac{1}{\omega_{eg} - \omega_3 - i\Gamma_{eg}} + \frac{1}{-\omega_{eg} - \omega_2 - i\Gamma_{eg}}\right)\right] \quad (25)$$

The expression for the susceptibility describing the scattering into the TG wave-vector-matching direction is given by $\chi^{(3)}(-\omega_s;\omega_1,-\omega_2,\omega_3)$.

In addition, for the 2D line shapes we set one of the frequencies equal to another as outlined in Table 1. For the six possible permutations of two independent frequencies and two wave-vector-matching conditions, there are two unique experiments. This observation arises from the symmetries displayed by eq 25. For $\omega_1 = \omega_2$, the 2D signal is independent of the wave-vector-matching geometry. This is readily seen from the equivalence of the scattered signal at $\omega_{PE} = -\omega_1 + \omega_2 + \omega_3$ and $\omega_{TG} = +\omega_1 - \omega_2 + \omega_3$ on exchange of the variables ω_1 and ω_2. The susceptibility for these experiments (cases IIIa and IVa) is given by

$$\chi^{(3)}_{TG}(\omega_1,\omega_3) = \frac{2}{\omega_1 - \omega_3 - i\Gamma_{ee}}\left[\left(\frac{1}{\omega_{eg} - \omega_3 - i\Gamma_{eg}}\right)^2 + \left[\frac{1}{\omega_{eg} - \omega_3 - i\Gamma_{eg}} + \frac{1}{-\omega_{eg} + \omega_1 - i\Gamma_{eg}}\right]\right] - \frac{\Gamma_{eg}}{\Gamma_{ee}}\frac{4}{\omega_{eg} - \omega_3 - i\Gamma_{eg}}\left(\frac{1}{(\omega_1 - \omega_{eg})^2 - \Gamma_{eg}^2}\right) \quad (26)$$

One can also see that the susceptibility for the PE signal with $\omega_1 = \omega_3$ is equal to the TG response for $\omega_2 = \omega_3$. From eq 26 it is also apparent that the exchange of ω_1 and ω_3 in this expression only leads to reflection of the 2D line shape about the diagonal axis. Therefore, functionally, cases IIIa, IIIb, IIIc, and IVb all lead to the same line shape.

The remaining cases are seen to be equal, since the PE signal for $\omega_2 = \omega_3$ is equal to the TG response for $\omega_1 = \omega_3$. For this case the susceptibility can be written as

$$\chi^{(3)}_{PE}(\omega_1,\omega_3) = \frac{4}{\omega_{eg} + \omega_1 - 2\omega_3 - i\Gamma_{eg}}\frac{1}{\omega_1 - \omega_3 - i\Gamma_{ee}}\left[\frac{1}{\omega_{eg} - \omega_3 - i\Gamma_{eg}} + \frac{1}{-\omega_{eg} + \omega_1 - i\Gamma_{eg}}\right] \quad (27)$$

We analyze the line shapes from the two experiments represented by cases IIIa and IVa, which are hereafter referred to by the wave-vector-matching condition as the PE and TG experiments, respectively. The 2D line shapes derived for these experiments from eqs 27 and 26 are plotted in Figure 7 for ratios of Γ_{eg}/Γ_{ee} varying from 1 to 10. For the PE experiment (Figure 7a−c), the line shape shows a clear signature of the Γ_{eg}/Γ_{ee} (T_1/T_2) ratio. When the vibrational dynamics are dominated by the population lifetime ($T_1 = 1/\Gamma_{ee}$), the contours of the line shape are oval, with a long axis that appears to be rotated clockwise by 15° from the diagonal axis. As the lifetime lengthens and the dynamics are dominated by pure-dephasing, the line shape becomes strongly elongated along the diagonal.

These observations are reflected in the slices through the 2D line shape. For the PE experiment, the slice along the diagonal axis has a width determined only by Γ_{eg}

$$S_-(\omega_-) = \frac{2}{((\omega_- - \omega_{eg})^2 + \Gamma_{eg}^2)^{3/2}}\frac{\Gamma_{eg}}{\Gamma_{ee}} \quad (28)$$

The antidiagonal slice is given by

$$S_+(\omega_+) = \frac{4}{[(9\omega_+^2 + \Gamma_{eg}^2)(\omega_+^2 + \Gamma_{eg}^2)(4\omega_+^2 + \Gamma_{ee}^2)]^{1/2}} \quad (29)$$

In the limit that $\Gamma_{ee} \ll \Gamma_{eg}$, the antidiagonal width is a Lorentzian with a width proportional to Γ_{ee}. These observations are illustrated in Figure 8a−c, which shows the diagonal and antidiagonal slices through the 2D line shapes in Figure 7a−c.

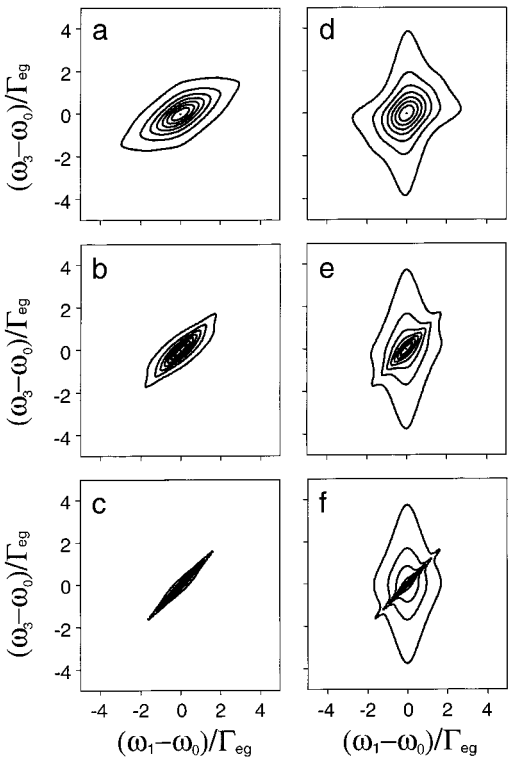

Figure 7. 2D line shapes, $S(\omega_1,\omega_3) \propto |\chi^{(3)}(\omega_1,\omega_3)|$, for a single 2LS from the frequency domain PE (a−c) and TG (d−f) experiments for (a, d) $\Gamma_{eg}/\Gamma_{ee} = 1$, (b, e) $\Gamma_{eg}/\Gamma_{ee} = 3$, and (c, f) $\Gamma_{eg}/\Gamma_{ee} = 10$.

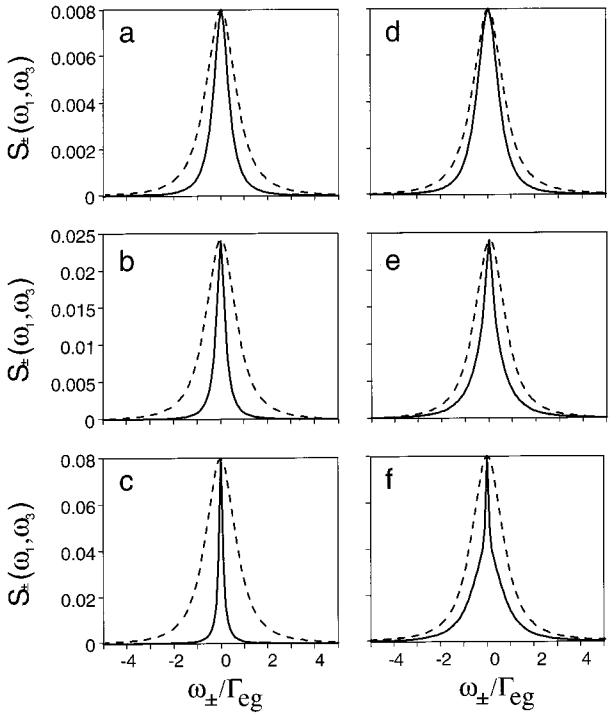

Figure 8. Diagonal (dashed line) and antidiagonal (solid line) slices through the 2D line shapes in Figure 7.

The line shapes obtained from the TG experiment for the same ratios of Γ_{eg}/Γ_{ee} are shown in Figure 7d−f. There are two clear contributions to this line shape. As seen from eq 26, the same line shape observed for the PE experiment exists in the TG experiment, but superimposed on an invariant contribution—the third term in eq 26. This pedestal has a diamond shape—an elongated 2D Lorentzian whose width in ω_1 is Γ_{eg} and in ω_3 is $2\Gamma_{eg}$. As the contribution of pure-dephasing to the line width increases, a strong diagonal ridge is observed on the diamond pedestal.

The dynamic information can also be obtained from slices through the 2D line shape. These are shown in Figure 8d−f. The diagonal slice for the TG is given by the same expression as the PE (eq 28). The antidiagonal slice is given by

$$S_+(\omega_+) = \frac{32(2\Gamma_{eg} - \Gamma_{ee})(\omega_+^2 + \Gamma_{eg}^2)^{1/2}}{[(4\omega_+^2 + \Gamma_{eg}^2)^{3/2}(16\omega_+^2 + \Gamma_{ee}^2)]^{1/2}} \quad (30)$$

For a line shape that is dominated by population relaxation ($\Gamma_{ee} \approx \Gamma_{eg}$), the antidiagonal slice is a Lorentzian line shape with a width of Γ_{eg}. As the contributions from pure-dephasing become more significant, a second feature is observed on top of this line shape, narrowing and growing in amplitude as Γ_{ee} approaches zero. In the limit $\Gamma_{ee} \ll \Gamma_{eg}$, this expression has two contributions: the invariant pedestal with width Γ_{eg} and a narrow spike of equal amplitude with width $2\Gamma_{ee}$.

Beyond these line shapes, it is of further importance to be able to extract the values of Γ_{ee} and Γ_{eg} from an inhomogeneous distribution.[36,40−42] The response for a system with inhomogeneous broadening is obtained by integration over a distribution function

$$\chi^{(3)} = \int G(\omega_{eg})\, \chi^{(3)}(\omega_{eg})\, d\omega_{eg} \quad (31)$$

Just as the time domain response from an inhomogeneous system can be written as the convolution of the homogeneous line shape integrated along the frequency diagonal, the addition of inhomogeneous broadening to the frequency domain calculations leads to integration over a distribution along the diagonal axis. With increased inhomogeneous broadening, line shapes for both experiments elongate along the diagonal. Yet for this distribution, the interpretation of the line shapes for the PE experiment becomes ambiguous. Slices along the diagonal or antidiagonal axes can potentially have contributions from Γ_{ee}, Γ_{eg}, and σ. This problem is not critical in the case of the TG experiment. Integration over the distribution still allows the value of Γ_{eg} and Γ_{ee} to be determined from an antidiagonal slice, whereas the diagonal slice is dictated by a convolution of the homogeneous and inhomogeneous widths (the 1D spectrum). What is observed for the coherent 2D line shapes is what is well-known from practice: the 2D experiments that are selective to inhomogeneous broadening are the PE in the time domain and the hole-burning experiment in the frequency domain. This statement is made recognizing that the TG experiment corresponds to a coherent hole-burning experiment—one in which coherent burning (ω_1) and reading (ω_3) beams are time coincident. If these beams are separated in time, the Γ_{ee} sensitive contributions disappear, leaving only the Γ_{eg} contributions.

Discussion

An intuitive description of 2D line shapes is important with increased complexity of the system. As the system to be investigated contains more and varying contributions from either spectroscopically distinct features or broadening of dynamic or structural origin, the description of the correlations between different frequency components will require models with a more advanced description of the system. This is particularly the case for vibrational spectroscopy, in which overlapping features from distinct transitions or from unique structural environments are standard. Examples of current interest include massive broadening of −OH stretch transitions in hydrogen-bonding liquids,[43−45] inhomogeneous broadening in supercooled liquids and glasses,[46]

and structurally distinct amide I vibrations in polypeptides.[22,24] 2D line shape analysis offers a powerful tool for examining such systems.

A traditional way of interpreting the observables from nonlinear optical spectroscopy is to define a model, calculate the form of the observable for certain parameters, and then make adjustment to parameters by comparing the experiment and model calculations. Particularly in the case of phenomenological models, there is little flexibility in this approach to assessing whether the model is appropriate for the system. A multidimensional observable is one that allows a more direct visualization of the dynamics of the system, and provides more direct feedback into the description of the system. At a qualitative level, a 2D spectrum can immediately distinguish between many different types of scenarios in a system with complex dynamics, and at a quantitative level, the full set of data in two time or frequency dimensions forms a tight constraint on any parametrization.

While several types of nonlinear optical problems can be interpreted within a 2LS model in which dynamics are described by Gaussian[47] or other[48] statistics, the tremendous power of 2D spectroscopy will be to unravel systems with an arbitrary number of degrees of freedom. The example in Figure 6 is a simple demonstration of how the 2D line shape can be used in evaluating a model. The variation of the dynamics within the ensemble as a function of frequency immediately suggests that a model based on a 2LS which experiences dynamics that follow Gaussian statistics would not truly represent this system. A traditional description of such a line shape using a 2LS coupled to a harmonic bath with arbitrary spectral density (i.e., a Brownian oscillator picture) would lead to an interpretation of a single transition coupled to a spectral density that includes frequency components spanning all of the members of the ensemble. The more appropriate picture is an ensemble of 2LSs each coupled to a bath oscillator with a spectral density of varying peak frequency. More precisely, recognizing that the 2D line shape is derived from a response that is a convolution of the individual response with a distribution function (eq 11), the 2D line shape can give insight into both the form of the distribution function and the individual response. While integrated time domain third-order nonlinear spectroscopies are not sensitive to the composition of the spectral density, the 2D versions of these experiments can reveal the presence of a heterogeneous bath.

Ultimately, realistic models of the 2D line shape must describe the dynamics of spectral diffusion and the manner in which the spectral density for these fluctuations manifests itself in these measurements. The measurement of spectral diffusion follows naturally from the time domain 2D experiments described above. The use of the τ_2 time variable in echo experiments will allow the dynamics of population relaxation and spectral diffusion to be monitored. The time evolution of the 2D line shape can be monitored as a function of the intermediate time variable, in a manner analogous to that of the spin diffusion experiment in NMR. Population relaxation (the Γ_{ee} and Γ_{gg} terms) will lead to decreased spectral amplitude, but no change in line shape. Spectral diffusion will lead to the shift of spectral amplitude off of the diagonal. The 2D line shape will vary from an inhomogeneously broadened line shape to one that is symmetric—apparently homogeneous—for values of τ_2 longer than those from the spectral diffusion dynamics.

Although related, this experiment should not be confused with a three-pulse photon echo peak shift measurement, which is used in the determination of a spectral density for the fluctuations of transitions that lie within the excitation bandwidth.[4,5,30] An analysis of this three-dimensional (3D) experiment will show that Fourier transform relationships involving τ_2 will lead to a 3D spectral density. This quantity will track the spectral density function for the time dependence of fluctuations between any two frequency components (ω_1 and ω_3) that lie within the excitation bandwidth. This quantity will be particularly important in describing strongly coupled multiple-state systems, whose electronic or vibrational dynamics are being increasingly studied.

In the case of frequency domain experiments, the inclusion of spectral diffusion complicates the analysis of the 2D line shape. The lack of resolution in time means that the integrated dynamics of spectral diffusion will be present in the 2D line shape. While static inhomogeneous broadening can certainly be discerned, the extraction of dynamics on multiple time scales from a 2D line shape will presumably suffer from the same difficulties as a 1D line shape analysis. Dynamics that appear vastly different in a time domain measurement often manifest themselves as subtle variations in the wings of a spectrum. The other possibility for addressing this problem and extracting frequency-resolved population dynamics is the judicious choice of tunable pulses with modest time and frequency resolution. This approach is being pursued in several forms, such as frequency-resolved resonant pump−probe spectroscopy,[22] frequency-selective or frequency-resolved photon echoes,[49,50] two-color photon echoes,[51] and infrared-pump incoherent anti-Stokes Raman probe experiments.[52,53]

In these calculations we have only addressed the absolute value line shape to demonstrate that significant information on the dynamics of the system can be obtained from 2D spectroscopies without the need for phase-sensitive detection. The time domain PE experiments above can be performed without the need for interferometric detection of the nonlinear signal. Yet, phase-sensitive detection will offer an even deeper level of characterization, in which both the information on amplitude (discussed above) and the phase of electronic and nuclear excitation are observed. This phase information can be shown to distinguish different anharmonic coupling mechanisms and interaction pathways in strongly coupled systems or chromophore aggregates.[15,20,54,55] In the case of phase-sensitive experiments, time-gated heterodyne detection[9,10] or spectral interferometry[33,34] are two approaches to this information.

Conclusions

Four types of 2D experiments based on time and frequency domain third-order nonlinear spectroscopies have been investigated to compare the information content of their 2D line shapes. The coherent signals scattered into two wave-vector-matched directions (PE and TG) are studied in the limits of high-time or high-frequency resolution.

The 2D line shape from the time domain PE measurement captures a complete description of the homogeneous dynamics, inhomogeneous broadening, and variation of the homogeneous dynamics within the ensemble. The diagonal slice contains the information of the traditional 1D absorption experiment, and the antidiagonal slice for a frequency Ω gives information on the homogeneous line shape of the subensemble at Ω. Inspection of 2D line shapes such as these is powerful for determining to what extent the standard models will truly represent this system.

Since 2D spectroscopy measures observables in two independent time or frequency variables, 2D techniques can always be related to three-point (or two-time-variable) correlation functions. On the other hand, it is clear from the time domain TG experiments that the converse is not always true; measure-

ment of a three-point correlation function does not necessarily imply a 2D spectroscopy.

Frequency domain experiments are selective to the ratio of rates for dephasing and population relaxation. In the case of static inhomogeneous broadening, the frequency domain TG experiment—a coherent hole-burning experiment—is sensitive to all of these variables. The prospects for using frequency domain experiments in complex systems will probably be reduced when models that include arbitrary spectral diffusion are included. Yet for time domain experiments, characterization of spectral diffusion naturally leads to a 3D experiment that probes the time evolution of the 2D line shape.

Acknowledgment. This work was started at the Technical University in Munich, for which A.T. thanks Professor Alfred Laubereau for his comments and helpful discussions, and the Alexander von Humboldt Foundation for a Research Fellowship. A.T. thanks Latham Boyle for assistance with the calculations and figures in the manuscript. This work was supported by the NSF (Grant CHE-9900342).

References and Notes

(1) Narasimhan, L. R.; Littau, K. A.; Pack, D. W.; Bai, Y. S.; Elschner, A.; Fayer, M. D. *Chem. Rev.* **1990**, *90*, 439.

(2) Koedijk, J. M. A.; Wannemacher, R.; Silbey, R. J.; Völker, S. *J. Phys. Chem.* **1996**, *100*, 19945.

(3) Meijers, H. C.; Wiersma, D. A. *Phys. Rev. Lett.* **1992**, *68*, 381.

(4) Cho, M.; Yu, J.-Y.; Joo, T.; Nagasawa, Y.; Passino, S. A.; Fleming, G. R. *J. Phys. Chem.* **1996**, *100*, 11944−11953.

(5) Joo, T.; Jia, Y.; Yu, J.-Y.; Lang, M. J.; Fleming, G. R. *J. Chem. Phys.* **1996**, *104*, 6089−6107.

(6) de Boeij, W.; Pshenichnikov, M. S.; Wiersma, D. A. *Chem. Phys. Lett.* **1996**, *253*, 53−60.

(7) Vöhringer, P.; Arnett, D. C.; Yang, T.-S.; Scherer, N. F. *Chem. Phys. Lett.* **1995**, *237*, 387.

(8) de Boeij, W. P.; Pshenichnikov, M. S.; Weirsma, D. A. *J. Phys. Chem.* **1996**, *100*, 11806−11823.

(9) de Boeij, W. P.; Pshenichnikov, M. S.; Wiersma, D. A. *Chem. Phys. Lett.* **1995**, *238*, 1−8.

(10) de Boeij, W. P.; Pshenichnikov, M. S.; Wiersma, D. A. *Chem. Phys. Lett.* **1995**, *247*, 264.

(11) Cho, M.; Fleming, G. R. *J. Phys. Chem.* **1994**, *98*, 3478.

(12) Joo, T.; Jia, Y.; Fleming, G. R. *J. Chem. Phys.* **1995**, *102*, 4063.

(13) Hybl, J. D.; Albrecht, A. W.; Gallager-Faeder, S. M.; Jonas, D. M. *Chem. Phys. Lett.* **1998**, *297*, 307.

(14) Zhang, W. M.; Chernyak, V.; Mukamel, S. Two-Dim Fs Spec of Coupled Chromophores. In *Ultrafast Phenomena XI*; Elsaesser, T. J. G. F., Wiersma, D., Zinth, W., Eds.; Springer-Verlag: Berlin, 1998; p 663.

(15) Zhang, W. M.; Chernyak, V.; Mukamel, S. *J. Chem. Phys.* **1999**, *110*, 5011.

(16) Tanimura, Y.; Mukamel, S. *J. Chem. Phys.* **1993**, *99*, 9496.

(17) Tominaga, K.; Yoshihara, K. *Phys. Rev. Lett.* **1995**, *171*, 179.

(18) Steffen, T.; Duppen, K. *Phys. Rev. Lett.* **1996**, *76*, 1224.

(19) Tokmakoff, A.; Fleming, G. R. *J. Chem. Phys.* **1997**, *106*, 2569.

(20) Tokmakoff, A.; Lang, M. J.; Larsen, D. S.; Fleming, G. R.; Chernyak, V.; Mukamel, S. *Phys. Rev. Lett.* **1997**, *79*, 2702.

(21) Cho, M. Two-Dimensional Vibrational Spectroscopy. In *Advances in Mulit-Photon Processes and Spectroscopy, Vol. 12*; Fujimura, Y., Lin, S. H., Eds.; World Scientific: Singapore, 1999; p 1.

(22) Hamm, P.; Lim, M.; Hochstrasser, R. M. *J. Phys. Chem. B* **1998**, *102*, 6123.

(23) Mukamel, S.; Piryatinski, A.; Chernyak, V. *Acc. Chem. Res.* **1999**, *32*, 145.

(24) Hamm, P.; Lim, M.; DeGrado, W. F.; Hochstrasser, R. M. *Proc. Natl. Acad. Sci. U.S.A.* **1999**, *96*, 2036.

(25) Okumura, K.; Tanimura, Y. *Chem. Phys. Lett.* **1998**, *295*, 298.

(26) Ernst, R. R.; Bodenhausen, G.; Wokaun, A. *Principles of Nuclear Magnetic Resonance in One and Two Dimensions*; Oxford University Press: Oxford, 1987.

(27) Okumura, K.; Tokmakoff, A.; Tanimura, Y. *Chem. Phys. Lett.*, in press.

(28) Mukamel, S. *Principles of Nonlinear Optical Spectroscopy*; Oxford University Press: New York, 1995.

(29) Bosma, W. B.; Yan, Y. J.; Mukamel, S. *Phys. Rev. A* **1990**, *42*, 6920.

(30) Fleming, G. R.; Cho, M. *Annu. Rev. Phys. Chem.* **1996**, *47*, 109−134.

(31) Hügel, W. A.; Heinrich, M. F.; Wegener, M.; Vu, Q. T.; Bányai, L.; Huag, H. *Phys. Rev. Lett.* **1999**, *83*, 3313.

(32) Lepetit, L.; Cheriaux, G.; Joffre, M. *J. Opt. Soc. Am. B* **1995**, *12*, 2467.

(33) Gallagher, S. M.; Albrecht, A. W.; Hybl, J. D.; Landin, B. L.; Rajaram, B.; Jonas, D. M. *J. Opt. Soc. Am. B* **1998**, *15*, 2338.

(34) Emde, M. F.; de Boeij, W. P.; Pshenichnikov, M. S.; Wiersma, D. A. *Opt. Lett.* **1997**, *22*, 1338.

(35) Bloembergen, N.; Lotem, H.; Lynch, R. T. *Indian J. Pure Appl. Phys.* **1978**, *16*, 151.

(36) Oudat, J.-L. *Phys. Rev. A* **1980**, *22*, 1141.

(37) Prior, Y. *IEEE J. Quantum Electron.* **1984**, *QE−20*, 37.

(38) Mukamel, S.; Loring, R. F. *J. Opt. Soc. B* **1986**, *3*, 595.

(39) Boyd, R. W. *Nonlinear Optics*; Academic Press: Boston, 1992.

(40) Druet, S. A. J.; Taran, J.-P. E.; Bordé, C. J. *J. Phys.* **1979**, *40*, 819.

(41) Carlson, R. J.; Wright, J. C. *J. Mol. Spectrosc.* **1990**, *143*, 1.

(42) Wright, J. C.; Chen, P. C.; Hamilton, J. P.; Zilian, A.; LaBuda, M. J. *Appl. Spectrosc.* **1997**, *51*, 949.

(43) Graener, H.; Seifert, G.; Laubereau, A. *Phys. Rev. Lett.* **1991**, *66*, 2092.

(44) Laenen, R.; Rauscher, C.; Laubereau, A. *Phys. Rev. Lett.* **1998**, *80*, 2622.

(45) Woutersen, S.; Emmerichs, U.; Bakker, H. J. *Science* **1997**, *278*, 658−60.

(46) Tokmakoff, A.; Fayer, M. D. *J. Chem. Phys.* **1995**, *103*, 2810.

(47) Kubo, R. A Stochastic Theory of Line-Shape and Relaxation. In *Fluctuation, Relaxation, and Resonance in Magnetic Systems*; Ter Haar, D., Ed.; Oliver and Boyd: London, 1962.

(48) Kubo, R.; Toyozawa, Y. *Prog. Theor. Phys.* **1955**, *13*, 160.

(49) Rector, K. D.; Zimdars, D.; Fayer, M. D. *J. Chem. Phys.* **1998**, *109*, 5455.

(50) Book, L. D.; Scherer, N. F. *J. Chem. Phys.* **1999**, *111*, 792.

(51) Yang, M. N.; Fleming, G. R. *J. Chem. Phys.* **1999**, *110*, 2983.

(52) Deak, J. C.; Iwaki, L. K.; Dlott, D. D. *J. Phys. Chem.* **1998**, *102*, 8193.

(53) Hofmann, M.; Graener, H. *Chem. Phys.* **1996**, *206*, 129.

(54) Okumura, K.; Tanimura, Y. *J. Chem. Phys.* **1997**, *107*, 2267.

(55) Chemyak, V.; Mukamel, S. *J. Chem. Phys.* **1998**, *108*, 5812.